Equilibrium thermodynamic theory explicitly including heat transport for evaluation of temperature distributions in steady plane-wave fronts

Cite as: Journal of Applied Physics **90**, 5576 (2001); https://doi.org/10.1063/1.1412827
Submitted: 30 July 2001 • Accepted: 23 August 2001 • Published Online: 13 November 2001

Tomokazu Sano and Yukio Sano

Equilibrium thermodynamic theory explicitly including heat transport for evaluation of temperature distributions in steady plane-wave fronts

Tomokazu Sano
Graduate School of Engineering, Osaka University, Suita, Osaka 565-0871, Japan

Yukio Sano[a)]
Kobe University of Mercantile Marine, Higashi-Nada-Ku, Kobe 658-0022, Japan

(Received 30 July 2001; accepted for publication 23 August 2001)

Previous theories that implicitly included heat transport predicted that temperatures were reduced in proportion to the viscous stresses in the whole region of an overdriven steady wave front in 2024 Al shocked at 80 GPa. Although there was a decrease in temperature caused by the shear stress, the decrease was very slight. A more justifiable theory that includes a heat transport term, the coefficient of which depends on the form and thickness of the effective part of a specific volume wave in the steady wave front, was then developed. The range of appropriate thicknesses of the effective part of the linear and sine forms for shocks up to 80 GPa in 2024 Al were determined. In these ranges, strain increments were sufficiently small and effective temperature rise-times were sufficiently long on the electron–phonon relaxation time scale to justify using equilibrium thermodynamics. In addition, the efficacy of the inside temperature method [Sano and Abe, J. Appl. Phys. **89**, 105 (2001)] was illustrated by evaluating heat transport. The inside temperature distribution can be specified if the thickness is measured because the distribution is not influenced to a great extent by the wave form.
 [DOI: 10.1063/1.1412827]

I. INTRODUCTION

Sano and Abe[1] developed the inside temperature (IT_{IM}) method implicitly including heat transport for estimating temperatures in steady wave fronts in a solid. Sano and Abe applied this method to shocks up to 140 GPa in yttria-doped tetragonal zirconia (YTZ) and evaluated the temperature distributions in multiple structure waves and overdriven shock waves. The evaluated temperatures behind the shocks were sufficiently correct and the evaluated inside temperature distributions were fairly correct. Therefore, the fundamental assumption of thermodynamic equilibrium and the assumption that heat transport and the work performed by thermal stress cancel each other out used in the IT_{IM} method were considered valid and the theory was deemed effective. Heat transport greatly reduced the temperatures in the rear of strong wave fronts and influenced inside temperature to a greater extent than does thermoelastic stress. Sano and Sano[2] evaluated the temperature distributions, effective strain rates, and effective temperature rise-times in overdriven steady wave fronts for shocks up to 80 GPa in 2024 Al, 250 GPa in Pt, and 230 GPa in Fe using the equilibrium thermodynamic theory (see Appendix A). This theory demonstrated that the IT_{IM} method was appropriate for the temperature distributions in wave fronts in metals for shocks up to 200–300 GPa. For those shocks, the effective strain increments were sufficiently small and the effective temperature rise-times were sufficiently long on the electron–phonon relaxation time scale for the fundamental assumption to be valid. The assumption of heat transport was also valid because the viscous stress component was sufficiently large compared with the thermal stress component. Thus, the efficacy of the IT_{IM} method and the accuracy of the inside temperature distributions were verified. In addition, evaluation of the temperature distributions in inviscid 2024 Al, Pt, and Fe solids indicated that viscous stress had a large influence. Here, an inviscid solid means a solid in which no viscous stress is induced during shock loading. Finally, the presence of the liquid phases in 2024 Al shocked at 80 GPa and in Pt shocked at 250 GPa, and intermediate melting states in Fe were examined. There was no liquid phase in 2024 Al and Pt. It was demonstrated that there might be a solid–liquid–solid Hugoniot for Fe. A series of a solid–liquid–solid Hugoniot and a liquid–solid Hugoniot, which is between a solid Hugoniot and a liquid Hugoniot, was estimated based on experimental data.

Despite the advances in the evaluation of inside temperature distributions, some questions remain as to the relation of the effect of viscosity to viscous stress and how to quantify the effect of shear stress. Further, it is important to develop a more justifiable theory for using equilibrium thermodynamics.

In the first half of the present study, we examined the effect of viscosity on the temperatures in an overdriven steady wave front in 2024 Al shocked at 80 GPa. For this purpose, the difference between the temperature in an inviscid solid and that in a solid (that is not inviscid), namely, the effect of viscosity, was formulated using the Mie–Grüneisen (MG) equation. Hereafter, a solid that is not inviscid is referred to as a noninviscid solid. The effect of viscosity was related to viscous stress by evaluating the ratio of the temperature difference to the viscous stress over the whole spe-

a)Electronic mail: sano@cc.kshosen.ac.jp

cific volume range. In addition, to examine the effect of shear stress, the minimum shear stress ($\tau_E=0$) partial solution of Wallace,[3,4] which is applicable to inviscid solids, was extended to be applicable to noninviscid solids. This effect was quantified by comparing the result with the temperature distribution obtained using the IT_{IM} method.

In the second half of the present study, we developed an equilibrium thermodynamic theory [inside temperature (IT_{EX}) method explicitly including heat transport] including a heat conduction term obtained using Fourier's law, which is more justifiable than the IT_{IM} method. The thickness of the effective part of the wave front (effective wave thickness) is determined such that the calculated temperature behind the wave front coincides with the temperature obtained using the Walsh–Christian (WC) equation[5] (see Appendix B). We evaluated temperature distributions in linear and sine effective-parts of overdriven steady wave fronts in 2024 Al for shocks up to 80 GPa in the ranges of appropriate effective-wave-thicknesses, together with effective wave and temperature rise-times. Both effective rise times indicated that the fundamental assumption is valid. Evaluation of heat transport indicated that the assumption of the transport used in the IT_{IM} method is valid. In addition, the influences of the wave form and thickness on the temperature and entropy distributions were determined.

II. EFFECTS OF VISCOUS AND SHEAR STRESSES

In this section, an equation for the difference between temperatures in inviscid and noninviscid solids is first derived from the MG equation. Next, the $\tau_E=0$ partial solution of Wallace is extended to be applicable to noninviscid solids. Finally, the effect of viscosity is related to viscous stress by evaluating the equation for the temperature difference and the effect of shear stress is examined quantitatively by comparing the $\tau_E=0$ partial solutions for inviscid and noninviscid solids.

A. Equation for temperature difference

The heat capacity at constant volume C_V used by Wallace[3,4] is given by the sum of a lattice and an electron part.

TABLE I. Input data for shock calculations in 2024 Al.[a]

Quality	2024 Al
T_0 (10^3 K)	0.293
ρ_0 (g/cm^3)	2.785
c (cm/μs)	0.533
s	1.338
γ_0	2.05
Γ_0 (10^{-4} cal/mole K^2)	3.30
g	1.8
κ (cal/cm s K)	0.48

[a]see Ref. 4.

$$C_V=3Nk+\Gamma T, \tag{1}$$

where T is temperature, N is the number of atoms per mole, k is the Boltzmann constant, and Γ is given by $\Gamma=\Gamma_0(V/V_0)^g$, where V is specific volume, and g, V_0, and Γ_0 are constants (see Table I). Subscript 0 refers to an ambient state. An equation for T is obtained by substituting Eq. (1) into the MG equation for thermal stress $\sigma_T=(\gamma_0/V_0)\int_0^T C_V dT$.[2]

$$T=\frac{-3Nk+\sqrt{(3Nk)^2+2\Gamma(V_0/\gamma_0)\sigma_T}}{\Gamma}, \tag{2}$$

where γ is the Grüneisen parameter, and $\gamma/V=\gamma_0/V_0$ was assumed. If Eq. (2) is applied to inviscid solids, then $T=T_{IV}$ and $\sigma_T=(\sigma_T)_{IV}$, while it is applied to noninviscid solids, then $T=T$ and $\sigma_T=\sigma_T$, where $(\sigma_T)_{IV}=\sigma-\sigma_C$ and $\sigma_T=\sigma_E-\sigma_C$, where σ is the stress on the Rayleigh line, σ_E is the thermoelastic stress, and σ_C is the cold stress. Subscript IV refers to an inviscid solid. σ_C is evaluated accurately using the WC equation. The following equation obtained from Eq. (2) indicates that the difference $(T_{IV}-T)$ depends on viscous stress $\sigma_v=\sigma-\sigma_E$.

$$T_{IV}-T=\frac{2(V_0/\gamma_0)\sigma_v}{\sqrt{(3Nk)^2+2\Gamma(V_0/\gamma_0)(\sigma_T)_{IV}}+\sqrt{(3Nk)^2+2\Gamma(V_0/\gamma_0)\sigma_T}}, \tag{3}$$

where $\sigma_T=(\sigma_E)_{IM}-\sigma_C$ is used for $\sigma_T=\sigma_E-\sigma_C$, and $\sigma_v=\sigma-(\sigma_E)_{IM}$ is used for $\sigma_v=\sigma-\sigma_E$, where $(\sigma_E)_{IM}$ is evaluated using the IT_{IM} method. σ is given by the Rayleigh line equation.

$$d\sigma=-\rho_0^2U_S^2dV, \tag{4}$$

where $\rho=1/V$ is the material density and U_S is the velocity of the wave front.

B. Minimum shear stress partial solution

Wallace[3] derived the $\tau_E=0$ partial solution that is applicable to inviscid solids. This solution is extended to be applicable to noninviscid solids. The extended solution is the solution of the equation expressed by

$$C_V\frac{dT}{dV}+\frac{\gamma_0}{V_0}C_VT=\frac{V_0}{\gamma_0}\left(\frac{dP_E}{dV}+B\rho\right), \tag{5}$$

where P_E is the thermoelastic pressure and B is the bulk

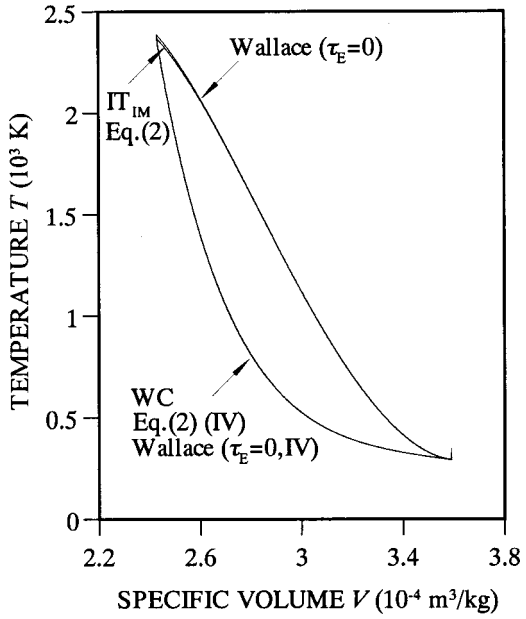

FIG. 1. Temperature distributions for the 80 GPa shock in 2024 Al obtained using Eq. (2) for noninviscid solids, IT_{IM} method, and Wallace's minimum shear stress ($\tau_E=0$) partial solution extended to be applicable to noninviscid solids. Distributions of temperature behind shocks up to 80 GPa obtained using Walsh–Christian (WC) equation, Eq. (2) for inviscid solids, and Wallace's $\tau_E=0$ partial solution are also shown.

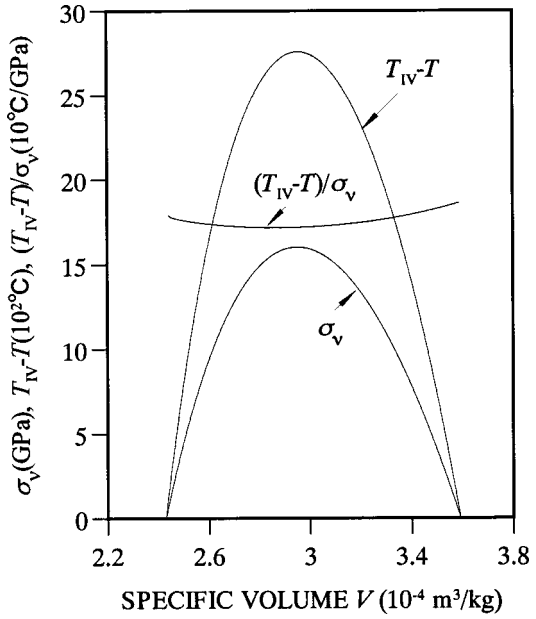

FIG. 2. Viscous stress σ_v-V, temperature difference $(T_{IV}-T)-V$, and ratio $(T_{IV}-T)/\sigma_v-V$ distributions for the 80 GPa shock in 2024 Al. Subscript IV refers to an inviscid solid.

modulus on the Rayleigh line defined by $B=-V\mathrm{d}P_S/\mathrm{d}V$, where P_S is the isentropic pressure. Here, we use an exact equation derived for B (see Appendix C).

$$B=-\frac{\gamma_0}{V_0}VT\left[-3Nk\left(\frac{\gamma_0}{V_0}\right)+\left(\frac{1}{2}\frac{d\Gamma}{dV}-\frac{\gamma_0}{V_0}\Gamma\right)T\right]-V\frac{dP_C}{dV}, \tag{6}$$

where cold pressure P_C is obtained correctly when the $\tau_E=0$ partial solution for inviscid solids is calculated. First, $(\sigma_E)_{IM}$ is used for P_E in Eq. (5) to calculate a $T-V$ relation in the wave front. A P_E-V relation is then calculated by the MG equation using the $T-V$ relation. Next, the sequence is repeated using the new P_E-V relation for P_E in Eq. (5) to obtain the $T-V$ and P_E-V relations. Each relation converges as the calculation is repeated.

C. Influence of viscous and shear stress

The data adopted by Wallace[3,4] for the calculations of shocks in 2024 Al, which are listed in Table I, were used here. Figure 1 shows temperature distributions in 2024 Al for the 80 GPa shock obtained using Eq. (2) for noninviscid solids, the IT_{IM} method, and the $\tau_E=0$ partial solution for noninviscid solids. The distribution obtained using noninviscid Eq. (2) was very close to that obtained using the IT_{IM} method: The temperature behind the shock was 2372.1 K for both cases. This is because the $(\sigma_E)_{IM}$ function was used for σ_E in Eq. (2). The distributions of temperature behind the shock up to the 80 GPa shock obtained using the WC equation, Eq. (2) for inviscid solids, and the $\tau_E=0$ partial solution for inviscid solids are shown in Fig. 1. Because inviscid Eq. (2) correctly evaluates the temperature behind the shock,[2] the distribution obtained using this equation was consistent with that obtained using the WC equation. On the other hand, the inviscid $\tau_E=0$ partial solution estimated higher temperatures behind the shocks than did the WC equation.

A previous study[2] revealed that the temperature distributions in inviscid 2024 Al, Pt, and Fe solids were overestimated. Here, this overestimate, namely, the effect of viscosity, was first related to viscous stress using Eq. (3). Γ is decreased monotonically, $(\sigma_T)_{IV}$ is decreased after it is increased, and σ_T is increased monotonically with a decrease in specific volume. As a result, if the denominator of Eq. (3) is constant, irrespective of specific volume, then the overestimate $(T_{IV}-T)$ is proportional to viscous stress σ_v. Figure 2 shows σ_v-V and $(T_{IV}-T)-V$ distributions for the 80 GPa shock calculated using the IT_{IM} method. Both distributions behaved similarly. A distribution of ratio $(T_{IV}-T)/\sigma_v$ is shown in Fig. 2. This distribution was essentially constant in the whole specific-volume range due to their similar behavior, indicating that the effect of viscosity is proportional to viscous stress to a good approximation. Thus, the temperature at a position in the wave front was reduced in proportion to the viscous stress at the same position.

Next, the noninviscid $\tau_E=0$ partial solution and the solution of noninviscid Eq. (2), which are shown in Fig. 1, were compared. The difference between both solutions represents the temperature reduction caused by shear stress. This difference was very slight, although it increased as specific volume decreased.

III. THEORY EXPLICITLY INCLUDING HEAT TRANSPORT

In this section, thermodynamic equations explicitly including heat transport, which can be solved properly, are first derived. These equations are applied to the effective parts of

specific volume waves in the wave fronts of linear and sine forms. We next present a criterion for appropriate temperature distributions and an equation for effective temperature thicknesses.

A. Thermodynamic equations

The increase in entropy $T\mathrm{d}S$ given by Sano *et al.*[1] takes the form.

$$TdS=-(\sigma-\sigma_{S_0})dV+dQ, \tag{7}$$

where Q is the heat transferred to the material, σ is the normal stress on the Rayleigh line, and σ_{S_0} is the isentropic stress $\sigma(V,S_0)$ that varies along an isentrope passing through the reference state. The continuity equation for heat transport in a steady wave front is expressed by $\mathrm{d}Q/\mathrm{d}Z=(\mathrm{d}J/\mathrm{d}Z)/(\rho_0 U_S)$, where $Z=X-U_S t$.[6] Here, X is the Lagrangian coordinate and t is time. The leading edge and the rear of the wave front are in a thermodynamic equilibrium state, so that heat flux J is $J_0=0$ at the leading edge and $J_\mathrm{H}=0$ at the rear, where subscript H refers to a state at the rear, namely a Hugoniot state. We obtain $Q-Q_0=J/(\rho_0 U_S)$ by integrating $\mathrm{d}Q=\mathrm{d}J/(\rho_0 U_S)$ from the leading edge to position Z in the wave front. Therefore, $Q_\mathrm{H}=Q_0$. Strain rate $\partial\varepsilon/\partial t$ is zero at the leading edge and the rear. Therefore, $\mathrm{d}V/\mathrm{d}Z=0$ and $\mathrm{dQ}/\mathrm{d}Z=\mathrm{d}J/\mathrm{d}Z=0$ at both ends.

Because the important process of heat transport is not the propagation of thermal energy, but heat conduction,[6,7] the constitutive equation for heat transport reduces to Fourier's law of heat conduction. The heat conduction equation is then expressed by $J=-\kappa(V_0/V)(\mathrm{d}T/\mathrm{d}Z)$, where κ is the thermal conductivity (see Table I), which is assumed to be constant.[4] For $\mathrm{d}V/\mathrm{d}Z\neq 0$, except for both ends of the wave front, the continuity equation is transformed as

$$dQ=-a\left(\frac{d^2T}{dV^2}-\frac{1}{V}\frac{dT}{dV}\right)dV, \tag{8}$$

where $a=(\kappa/\rho_0 U_S)(V_0/V)(\mathrm{d}V/\mathrm{d}Z)$. From Eqs. (7) and (8)

$$dS=-\frac{1}{T}\left(\sigma-\sigma_{S_0}+a\frac{d^2T}{dV^2}-\frac{a}{V}\frac{dT}{dV}\right)dV. \tag{9}$$

By equating Eq. (9) with thermodynamic identity $TdS=C_V dT+C_V(\gamma_0/V_0)TdV$, we obtain a thermodynamic equation that explicitly includes heat transport, which is expressed by

$$a\frac{d^2T}{dV^2}+\left(C_V-\frac{a}{V}\right)\frac{dT}{dV}+\frac{\gamma_0}{V_0}C_V T=-(\sigma-\sigma_{S_0}). \tag{10}$$

The above equation can be solved under the boundary conditions that $T=T_0$ at V_0 and $T=T_\mathrm{H}$ at V_H. Because coefficient a includes $\mathrm{d}V/\mathrm{d}Z$, information on the real specific-volume wave is necessary for determining $\mathrm{d}V/\mathrm{d}Z$. Here, however, we determine what can be learned about the influence of heat transport on the temperature distribution without using any real wave forms. The specific-volume $V(\overline{Z})$ wave in a real overdriven-steady-wave front with thickness h is shown schematically in Fig. 3(a). Because $\mathrm{d}V/\mathrm{d}\overline{Z}=0$ at the leading edge as described above, the slope in the front zone

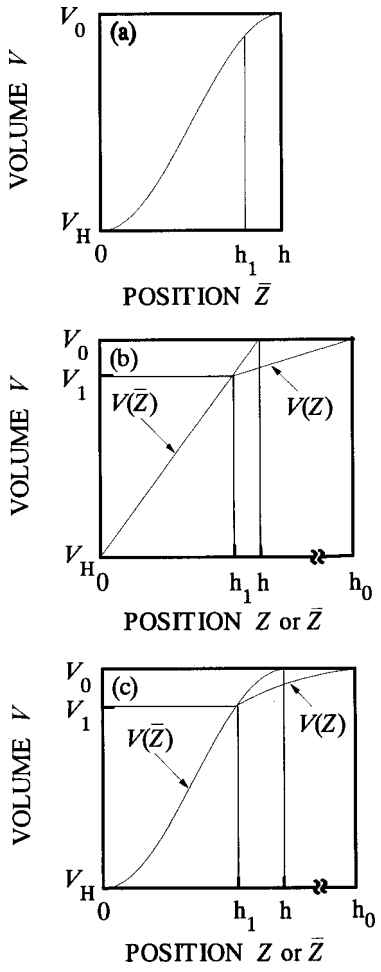

FIG. 3. Schematic diagrams of (a) a real overdriven $V(\overline{Z})$ wave of thickness h, (b) a linear $V(\overline{Z})$ wave of effective thickness h and a linear $V(Z)$ wave of thickness h_0 with an extended front zone (h_0-h_1), and (c) a sine$V(\overline{Z})$ wave of effective thickness h and a sine$V(Z)$ wave of thickness h_0 with an extended front zone (h_0-h_1).

$(h_1\leqslant\overline{Z}\leqslant h)$ of the $V(\overline{Z})$ wave is gradual. We consider a $V(Z)$ wave in which this front zone with a gradual slope is extended to $h_1\leqslant Z\leqslant h_0$. The front zone of the $V(Z)$ wave from $Z=h_1$ to $Z=h_0$ must be sufficiently long for Eq. (10), which includes the heat conduction term obtained using Fourier's law, to be solved properly. To obtain information regarding a in the front zone, a is rewritten using a transformation function $\overline{Z}=f(Z)$.

$$a=\frac{\kappa}{\rho_0 U_S}\frac{V_0}{V}\frac{df}{dZ}\frac{dV}{d\overline{Z}}. \tag{11}$$

In $0\leqslant Z\leqslant h_1$, $\mathrm{d}f(Z)/\mathrm{d}Z=1$ or $f(Z)=Z$. In the front zone of $h_1<Z\leqslant h_0$, for the sake of simplicity, we use $\mathrm{d}f(Z)/\mathrm{d}Z=\alpha$ or $f(Z)=\alpha Z+(1-\alpha)h_1$, where $\alpha=(h-h_1)/(h_0-h_1)$. It follows from $\mathrm{d}\overline{Z}/\mathrm{d}Z\ll 1$ that $h\ll h_0$. Therefore, it might be assumed that $\alpha=0$ and $a=0$ or $\mathrm{d}Q=0$ in the front zone. This is tantamount to assuming that $\mathrm{d}Q=0$ in the front zone from $\overline{Z}=h_1$ to $\overline{Z}=h$. Then, Eq. (10) reduces to

$$C_V\frac{dT}{dV}+\frac{\gamma_0}{V_0}C_V T=-(\sigma-\sigma_{S_0}). \tag{12}$$

The above equation holds, independent of the form of the specific volume wave in the front zone.

Here, the analysis is performed for two typical $V(\overline{Z})$ waves of effective thickness h to examine the influence of the wave form on the temperature distribution in the wave front. One is a linear $V(\overline{Z})$ wave, which is shown together with the corresponding linear $V(Z)$ wave in Fig. 3(b), while the other is a sine $V(\overline{Z})$ wave, which is shown together with the corresponding sine $V(Z)$ wave in Fig. 3(c). The $V(Z)$ waves require sufficiently wide front-zones to properly perform the calculations illustrated below.

1. Linear wave

The linear $V(\overline{Z})$ wave is expressed by

$$V = V_H + \frac{V_0 - V_H}{h}\overline{Z}, \tag{13}$$

where h is the effective thickness of the linear wave. For this wave, Eq. (11) becomes

$$a = \frac{\kappa}{\rho_0 U_S}\frac{V_0}{V}\frac{V_0 - V_H}{h}. \tag{14}$$

We used Eq. (12) from h_0 to h_1 or from V_0 to V_1 and Eq. (10) with Eq. (14) from h_1 to 0 or from V_1 to V_H. These two equations were solved using the difference method. The calculation was begun from V_0 and proceeded toward V_H. This method for estimating temperatures in the linear wave is referred to as an inside temperature ($\mathrm{IT_{EXL}}$) method explicitly including heat transport.

2. Sine wave

The sine $V(\overline{Z})$ wave is expressed by

$$V = \frac{1}{2}\left[(V_0 + V_H) - (V_0 - V_H)\cos\left(\pi\frac{\overline{Z}}{h}\right)\right], \tag{15}$$

where h is the effective thickness of the sine wave. For the sine wave

$$a = \frac{\pi}{2}\frac{\kappa}{\rho_0 U_S}\frac{V_0}{V}\frac{V_0 - V_H}{h}\sin\left(\pi\frac{\overline{Z}}{h}\right), \tag{16}$$

where $\sin(\pi\overline{Z}/h) = 2\sqrt{(\varepsilon/\varepsilon_H)(1-\varepsilon/\varepsilon_H)}$, where $\varepsilon = 1 - V/V_0$. Equation (12) was used from V_0 to V_1, Eq. (10) with Eq. (16) was used from V_1 to V_H, and the calculation proceeded toward V_H from V_0. This method for estimating the temperatures in the sine wave is referred to as an inside temperature ($\mathrm{IT_{EXS}}$) method.

B. Criterion of temperature distributions

The calculated temperature behind the linear wave for shock loading can be fitted to the temperature behind the shock obtained accurately using the WC equation if effective wave thickness h and ratio h_1/h are chosen appropriately. For any values of h used, however, if h_1/h is greater than $(h_1)_{\mathrm{cru}}/h_{\min}$, where $h_{\min}$ refers to a minimum value of h, the fitting is impossible because the calculated temperature at the rear never rises to the temperature behind the shock. For appropriate thicknesses h and appropriate ratios h_1/h between $(h_1)_{\mathrm{cru}}/h_{\min}$ and $(h_1)_{\mathrm{crl}}/h_{\max}$, where $h_{\max}$ refers to a maximum value of h, the calculated temperatures increase monotonically to the temperature behind the shock with a decrease in specific volume. If ratio h_1/h is smaller than $(h_1)_{\mathrm{crl}}/h_{\max}$, then the calculated temperature reaches the temperature behind the shock at a specific volume, has a peak between the specific volume and V_H, and then decreases monotonically, and approaches the temperature behind the shock at V_H. Because $\mathrm{d}T/\mathrm{d}V \leqslant 0$, as revealed by Wallace,[4] the temperature distribution including a portion where $\mathrm{d}T/\mathrm{d}V > 0$ is inappropriate. Therefore, the criterion for appropriate temperature distributions is given by the inequality

$$\frac{(h_1)_{\mathrm{crl}}}{h_{\max}} \leqslant \frac{h_1}{h} \leqslant \frac{(h_1)_{\mathrm{cru}}}{h_{\min}}. \tag{17}$$

The above inequality indicates that there is an effective wave-thickness range ($h_{\min} \leqslant h \leqslant h_{\max}$) for shock loading and that there is an upper temperature distribution boundary at $(h_1)_{\mathrm{crl}}/h_{\max}$, where the distribution is $\mathrm{d}T/\mathrm{d}V = 0$ at V_H, and the lower boundary at $(h_1)_{\mathrm{cru}}/h_{\min}$. The same is true of the sine wave.

C. Effective temperature thickness

Effective temperature thickness ΔZ is given by[2,4]

$$\Delta Z = \frac{\kappa(T_H - T_0)}{\{(1-\varepsilon)J\}_{\max}}. \tag{18}$$

The equation for heat flux is obtained from the continuity equation for heat transport.[2]

$$J = U_S(\varepsilon_H - \varepsilon)\frac{dQ}{dV}, \tag{19}$$

where $\mathrm{d}Q/\mathrm{d}V$ is given by Eq. (8). Quantity $\{(1-\varepsilon)J\}_{\max}$ in Eq. (18) is determined by incorporating Eq. (19) into the $\mathrm{IT_{EXL}}$ and $\mathrm{IT_{EXS}}$ methods.

IV. ASSUMPTIONS OF THERMODYNAMIC EQUILIBRIUM AND HEAT TRANSPORT

Ratios $(h_1)_{\mathrm{cru}}/h_{\min} = 0.57$ and $(h_1)_{\mathrm{crl}}/h_{\max} = 0.43$ for the 80 GPa shock ($\varepsilon_H = 0.324$) were obtained using the $\mathrm{IT_{EXL}}$ method. Effective wave thicknesses h, effective temperature thicknesses ΔZ, effective wave rise-times Δt_s, and temperature rise-times Δt for several $(1-h_1/h)$ in the range of $0.43 \leqslant 1-h_1/h \leqslant 0.57$ are listed in Table II, where $\Delta t_s = h/U_S$ and $\Delta t = \Delta Z/U_S$, where $U_S = 9409$ m/s for the 80 GPa shock. The wave thickness increased with an increase in $(1-h_1/h)$ from 0.19×10^{-8} m at $(1-h_1/h) = 0.43$ to 5.2×10^{-8} m at $(1-h_1/h) = 0.57$, while the temperature thickness increased from 5.8×10^{-8} m at 0.43 to 7.9×10^{-8} m at 0.57. Calculations were also performed for the 20, 40, and 60 GPa shocks ($\varepsilon_H = 0.1575, 0.2364, 0.2873$). Quantities h, ΔZ, and Δt for $1-(h_1)_{\mathrm{cru}}/h_{\min}$, $1-(h_1)_{\mathrm{crl}}/h_{\max}$, and an intermediate value between them are listed in Table III. Both effective wave and temperature rise-times decreased with an increase in shock loading for the same value of $(1-h_1/h)$. For the 80 GPa shock, the effective wave rise-times were between 0.21×10^{-12} and 0.55×10^{-11} s and the effective

TABLE II. Effective wave thicknesses h, effective temperature thicknesses ΔZ, effective wave rise-times Δt_s, and effective temperature rise-times Δt for $1-(h_1)_{\mathrm{cru}}/h_{\min}$, $1-(h_1)_{\mathrm{crl}}/h_{\max}$, and several $1-h_1/h$ between them calculated using the $\mathrm{IT_{EXL}}$ and $\mathrm{IT_{EXS}}$ methods for the 80 GPa shock in 2024 Al, respectively.

	Linear waves				Sine waves			
$1-h_1/h$	$h\times10^8$ (m)	$\Delta Z\times10^8$ (m)	$\Delta t_s\times10^{11}$ (s)	$\Delta t\times10^{11}$ (s)	$h\times10^8$ (m)	$\Delta Z\times10^8$ (m)	$\Delta t_s\times10^{11}$ (s)	$\Delta t\times10^{11}$ (s)
0.43	0.1945	5.791	0.0207	0.6155	0.2660	5.8060	0.0283	0.6171
0.44	0.4675	5.905	0.0497	0.6276	0.6360	5.9440	0.0676	0.6317
0.45	0.75	6.025	0.0797	0.6403	1.0140	6.0900	0.1078	0.6473
0.46	1.0420	6.1510	0.1107	0.6537	1.399	6.2460	0.1487	0.6638
0.47	1.345	6.282	0.1429	0.6677	1.792	6.411	0.1905	0.6814
0.48	1.659	6.419	0.1763	0.6822	2.195	6.587	0.2333	0.7001
0.49	1.986	6.561	0.2111	0.6973	2.608	6.774	0.2772	0.7199
0.50	2.327	6.710	0.2473	0.7131	3.031	6.974	0.3221	0.7412
0.51	2.683	6.865	0.2851	0.7296	3.465	7.185	0.3683	0.7636
0.52	3.055	7.026	0.3246	0.7467	3.911	7.411	0.4157	0.7877
0.53	3.444	7.193	0.3660	0.7645	4.370	7.651	0.4644	0.8132
0.54	3.852	7.367	0.4094	0.7830	4.844	7.905	0.5148	0.8402
0.55	4.282	7.545	0.4551	0.8019				
0.56	4.734	7.729	0.5031	0.8214				
0.57	5.211	7.918	0.5538	0.8415				

strain rates were on the order of $10^{11}\,\mathrm{s}^{-1}$ except for in the neighborhood of $1-(h_1)_{\mathrm{cru}}/h_{\min}=0.43$. The electron–phonon relaxation times, which are dominant for shocks up to 200–300 GPa in metals, are on the order of 10^{-14} s. Consequently, the strain increases during the relaxation times are only on the order of 10^{-3}. On the other hand, the temperature rise times between 0.62×10^{-11} and 0.84×10^{-11} s for the 80 GPa shock are sufficiently long compared with the electron–phonon relaxation times. Therefore, the fundamental assumption is valid for shocks up to 80 GPa.

Figure 4 shows a temperature distribution in the linear wave for $1-h_1/h=0.49$ in the case of the 80 GPa shock, together with that calculated using the $\mathrm{IT_{IM}}$ method. Both distributions coincided comparatively well. This demonstrates that the $\mathrm{IT_{IM}}$ method is effective. To further demonstrate its efficacy, $\mathrm{d}W^{\mathrm{v}}=-\sigma_{\mathrm{v}}\mathrm{d}V$, $\mathrm{d}W^{\mathrm{h}}=-(\sigma_E-\sigma_{S_0})\mathrm{d}V$, and $\mathrm{d}Q_L=-a\{\mathrm{d}^2T/\mathrm{d}V^2-(1/V)\mathrm{d}T/\mathrm{d}V\}\mathrm{d}V$, where $\mathrm{d}V=(V_0-V_H)/100$, for $1-h_1/h=0.49$, are calculated using the $\mathrm{IT_{EXL}}$ method and are shown in Fig. 5. $\mathrm{d}W^{\mathrm{v}}\gg\mathrm{d}W^h+\mathrm{d}Q_L$ except for in the neighborhood of V_H. This is the primary evidence of the efficacy of the $\mathrm{IT_{IM}}$ method.

Figure 6 shows the lower and upper boundaries of the distributions obtained for $1-(h_1)_{\mathrm{cru}}/h_{\min}=0.43$ and $1-(h_1)_{\mathrm{crl}}/h_{\max}=0.57$, respectively. Both curves are similar. The curves shifted continuously from the lower curve to the upper curve with an increase in $(1-h_1/h)$. The distribution obtained using the $\mathrm{IT_{IM}}$ method is shown in Fig. 6. This distribution was estimated lower, because the assumption $\mathrm{d}Q=-\mathrm{d}W^h<0$ was used in the whole range of specific volume in the $\mathrm{IT_{IM}}$ method, despite the fact that $\mathrm{d}Q\cong0$ in the larger specific volume range.

Ratios $(h_1)_{\mathrm{cru}}/h_{\min}=0.57$ and $(h_1)_{\mathrm{crl}}/h_{\max}=0.46$ for the 80 GPa shock were obtained using the $\mathrm{IT_{EXS}}$ method. Quantities h, ΔZ, Δt_s, and Δt for several $(1-h_1/h)$ are listed in Table II. Both thicknesses also increased with an increase in $(1-h_1/h)$ in this case. The quantities for the 20, 40, 60 GPa shocks are listed in Table III. At the same value of $(1-h_1/h)$ for each shock, the strain increment in the relaxation time is only slightly larger and the effective temperature rise-time is longer for the sine wave, and therefore, the fundamental assumption is also valid for this wave. In addition, the dQ_S distribution for $1-h_1/h=0.49$, which was cal-

TABLE III. Effective wave thicknesses h, effective temperature thicknesses ΔZ, effective wave rise-times Δt_s, and effective temperature rise-times Δt for $1-(h_1)_{\mathrm{cru}}/h_{\min}$, $1-(h_1)_{\mathrm{crl}}/h_{\max}$, and an intermediate value calculated using the $\mathrm{IT_{EXL}}$ and $\mathrm{IT_{EXS}}$ methods for the 20, 40, and 60 GPa shocks in 2024 Al, respectively.

Shocks		Linear waves					Sine waves			
(GPa)	$1-h_1/h$	$h\times10^8$ (m)	$\Delta Z\times10^8$ (m)	$\Delta t_s\times10^{11}$ (s)	$\Delta t\times10^{11}$ (s)	$1-h_1/h$	$h\times10^8$ (m)	$\Delta Z\times10^8$ (m)	$\Delta t_s\times10^{11}$ (s)	$\Delta t\times10^{11}$ (s)
	0.42	0.2150	6.8120	0.025	0.7866	0.42	0.2990	6.8540	0.035	0.7915
60	0.50	2.947	8.265	0.3403	0.954	0.48	2.906	8.100	0.336	0.935
	0.59	7.499	10.570	0.8660	1.221	0.54	5.950	9.999	0.6871	1.155
	0.41	0.2880	8.9670	0.033	1.0355	0.41	0.4080	8.9680	0.047	1.0356
40	0.50	3.906	11.670	0.4510	1.348	0.48	4.024	11.380	0.4647	1.315
	0.60	10.46	16.45	1.2079	1.90	0.55	8.468	15.530	0.9779	1.79
	0.41	0.5160	17.6500	0.076	2.6142	0.41	0.7550	17.7900	0.112	2.6345
20	0.51	6.024	26.520	0.8921	3.93	0.49	6.450	25.450	0.9552	3.77
	0.62	19.06	47.98	2.8225	7.10	0.58	16.00	48.80	2.3694	7.23

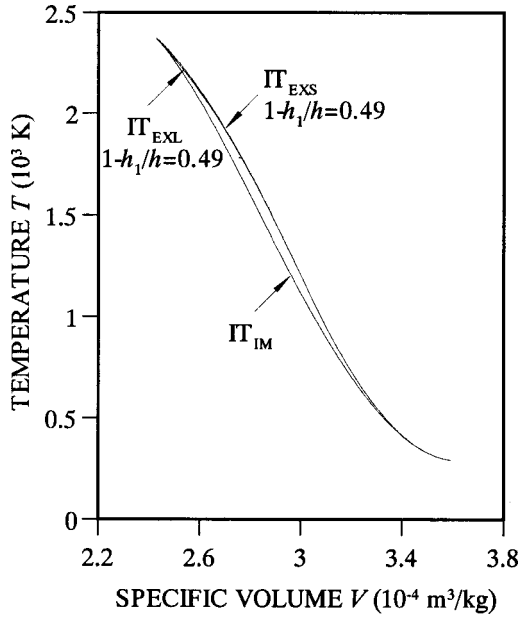

FIG. 4. Temperature distributions for $1-h_1/h=0.49$ calculated using the IT_{EXL}, IT_{EXS}, and IT_{IM} methods for the 80 GPa shock in 2024 Al.

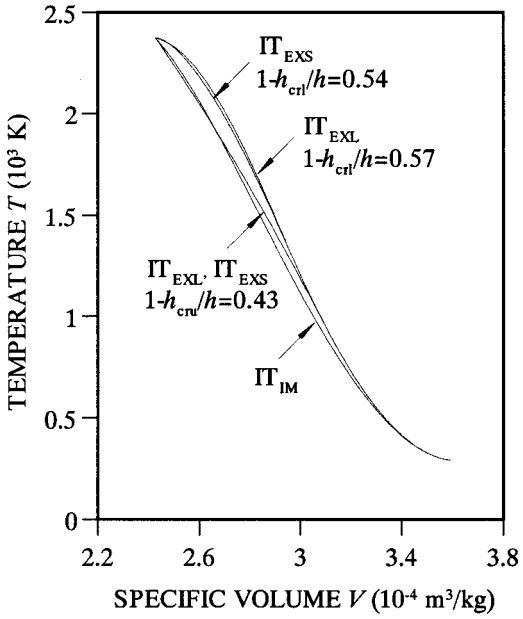

FIG. 6. Upper and lower boundaries of temperature distributions calculated using the IT_{EXL} and IT_{EXS} methods for the 80 GPa shock in 2024 Al.

culated using the IT_{EXS} method and shown in Fig. 5, is close to the dQ_L distribution. This also demonstrates the efficacy of the IT_{IM} method. The lower and upper boundaries of the distributions in the sine wave are shown in Fig. 6. Both boundaries are closer for the sine wave.

V. INFLUENCES OF WAVE FORM AND THICKNESS

A. Temperature distributions

For any $(1-h_1/h)$, as listed in Table II, the effective thickness of the linear wave was approximately equal to that of the sine wave and, as shown in Fig. 4, both temperature distributions coincided well except for in the neighborhood of V_H. Near V_H, the distribution was a little lower for the linear wave. In Eqs. (10) and (12), used for estimating the temperatures, only coefficient a depends on the wave form. Therefore, the difference in temperature was caused by dQ. Because $|dQ_L|$ increased more than $|dQ_S|$ with a decrease in specific volume as shown in Fig. 5, the temperature rose with a slower speed for the linear wave. For any $(1-h_1/h)$, however, $|(dQ_L-dQ_S)/dQ_L|$ was sufficiently small in the whole specific volume range, as was the case with Fig. 5. Furthermore, in the case where both thicknesses were similar, the temperature distributions also coincided well. The same was true of the 20, 40, 60 GPa shocks. Thus, for shocks up to 80 GPa, the wave form barely influenced the temperature distribution.[8] In contrast, the thickness greatly influenced the temperature distribution. Consequently, the temperature distribution can be specified if the thickness is measured by a shock experiment. This is very advantageous because it is difficult to experimentally measure the distribution accurately.

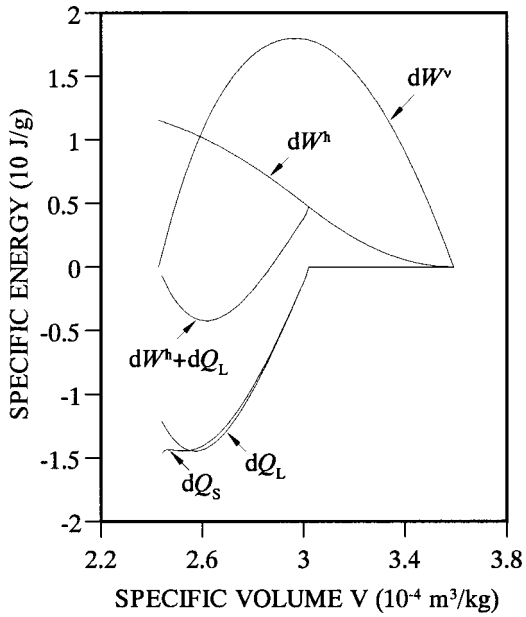

FIG. 5. dW^v-V, dW^h-V, and $(dW^h+dQ_L)-V$ distributions for $1-h_1/h=0.49$ calculated using the IT_{EXL} method and dQ_S-V distribution calculated using the IT_{EXS} method for the 80 GPa shock in 2024 Al.

B. Entropy distributions

Figure 7 shows the $(S-S_0)$ distribution for $1-h_1/h=0.49$ in the case of the 80 GPa shock calculated using the IT_{EXL} method. The change in entropy is explained using Eq. (7) and Fig. 5. Entropy is increased with a decrease in specific volume by work $dW=dW^h+dW^v=-(\sigma-\sigma_{S_0})dV$ in the whole specific-volume region and heat transport $dQ>0$ from V_0 to V_1. Because $dQ\cong 0$ from V_0 to V_1, however, the influence of dQ is very slight. On the other hand, the rate of increase in entropy is reduced by the increase in the temperature in the wave front T in the whole specific-volume and by $dQ<0$ from V_1 to V_H. The same is true of the entropy distribution in the sine wave. A similar distribution was obtained using the IT_{EXS} method (Fig. 7). The reason for this is

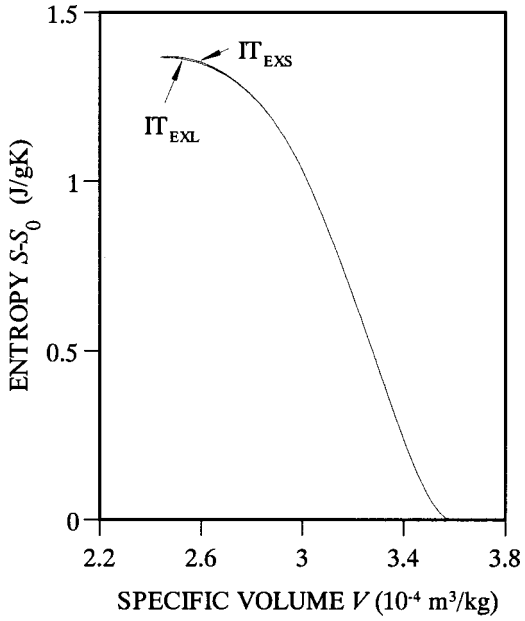

FIG. 7. Entropy distributions for $1-h_1/h=0.49$ calculated using the IT_{EXL} and IT_{EXS} methods for the 80 GPa shock in 2024 Al.

that the difference in T between both waves was very slight, there was no difference in dW, and the difference in dQ was sufficiently small compared with dQ itself, as described above. In short, even near V_H, where the difference in dQ is greatest, dS differed only slightly. Furthermore, in the case where both thicknesses were similar, the entropy distributions also coincided well. Thus, the wave form barely influenced the entropy distribution.

C. Values of α

Without assuming $\alpha=0$, that is, using only Eq. (10), the value of α was estimated for the linear wave. The temperature behind the shock for $1-h_1/h=0.49$ was 2374.3 K with $\alpha \leqslant 1.1\times10^{-4}$ and $h_0 \geqslant 1.2\times10^{-4}$ m. Because 1.1×10^{-4} is nearly zero, the temperature distributions for $\alpha \leqslant 1.1\times10^{-4}$ coincided very well with that for $\alpha \cong 0$ calculated above. For $1-h_1/h=0.49$ in the case of the sine wave, the temperature behind the shock was 2374.3 K with $\alpha \leqslant 1.8\times10^{-4}$ and $h_0 \geqslant 1.0\times10^{-4}$ m.

VI. CONCLUSIONS

In the first half of the present study, the effects of viscous and shear stresses on the temperature distribution in the overdriven steady wave front in 2024 Al shocked at 80 GPa were examined using theories that implicitly include heat transport. The inside temperatures decreased greatly in proportion to the viscous stresses, but were reduced only slightly by the shear stresses. In the second half, a more justifiable theory that explicitly includes heat transport was developed. The temperature distributions were evaluated in the range of the appropriate effective thicknesses of linear and sine specific-volume waves, together with the effective wave and temperature rise-times. The effective strain increments that were estimated using the effective wave rise-times were sufficiently small and the effective temperature rise-times were sufficiently long on the electron–phonon relaxation scale for the assumption of thermodynamic equilibrium to be valid. The primary evidence demonstrating that the inside temperature (IT_{IM}) method is effective was obtained by evaluating heat transport. In addition, it was clarified that the wave form did not influence the temperature distributions to a great extent. Therefore, the temperature distribution can be specified after the wave thickness has been determined.

APPENDIX A: EQUILIBRIUM THERMODYNAMIC THEORY (IT_{IM} METHOD)

Sano and Abe[1] derived the following irreversible thermodynamic equation by assuming that heat transport and the work performed by the thermal stress could cancel each other out.

$$C_V\frac{dT}{dV}+\frac{\gamma_0}{V_0}C_VT=-(\sigma-\sigma_E), \tag{A1}$$

where σ is a known Rayleigh-line-stress function $\sigma(V)$. A set of equations used in the IT_{IM} method consists of Eq. (A1), the equation for cold stress σ_C, and the equation for thermoelastic stress σ_E. The equation for σ_C is given by

$$\sigma_C=\sigma_H-\sigma_{T_H}, \tag{A2}$$

where σ_H is a known Hugoniot function for normal stress $\sigma_H(V)$ and σ_{T_H} is a Hugoniot function for thermal stress $\sigma_{T_H}(V)$ expressed by

$$\sigma_{T_H}=\frac{\gamma_0}{V_0}\int_0^{T_H}C_V dT.$$

The equation for σ_E is given by

$$\sigma_E=\sigma_C+\sigma_T, \tag{A3}$$

where σ_T is the thermal stress expressed by

$$\sigma_T=\frac{\gamma_0}{V_0}\int_0^{T}C_V dT.$$

Equations (A1)–(A3) were calculated by the iterative method using the Hugoniot function and the Rayleigh-line-stress function to determine the temperature, cold compression curve, and thermoelastic stress.

Sano and Sano[2] derived the following equation using Eq. (A1).

$$C_{VH}\frac{dT_H}{dV_H}+C_{VH}\frac{\gamma_0}{V_0}T_H=\left(1+\frac{\Gamma_H T_H}{3Nk}\right)\left\{\frac{1}{2}\frac{d\sigma_H}{dV_H}(V_0-V_H)+\frac{1}{2}(\sigma_H-\sigma_0)\right\}. \tag{A4}$$

The above equation is close to the WC equation [see Eq. (B1)] for shocks up to 200–300 GPa in metals because $\Gamma T/3Nk \ll 1$. Thus, they demonstrated that the IT_{IM} method is a reasonable approximation to the standard method

APPENDIX B: WALSH AND CHRISTIAN THEORY

The thermodynamic equilibrium equation derived by Walsh and Christian[5] is

$$C_V\frac{dT}{dV}+\frac{\gamma_0}{V_0}C_VT=\frac{1}{2}\frac{d\sigma}{dV}(V_0-V)+\frac{1}{2}(\sigma-\sigma_0), \quad \text{(B1)}$$

where C_V,σ,T,V are the quantities in a Hugoniot function.

APPENDIX C: BULK MODULUS

Bulk modulus is defined by

$$B=-V\frac{dP_S}{dV}, \quad \text{(C1)}$$

where $dP_S/dV\equiv(\partial P/\partial V)_S$. The isentropic pressure P_S is given as the sum of the cold pressure P_C and the isentropic thermal pressure P_{T_S}.

$$P_S=P_C+P_{T_S}, \quad \text{(C2)}$$

where

$$P_{T_S}=\frac{\gamma_0}{V_0}\int_0^{T_S}C_V dT,$$

where T_S is the isentropic temperature and we have assumed that $\gamma/V=\gamma_0/V_0$. By substituting Eq. (1) into the above equation

$$P_{T_S}=\frac{\gamma_0}{V_0}\left(3NkT_S+\frac{1}{2}\Gamma T_S^2\right), \quad \text{(C3)}$$

where T_S is expressed by

$$T_S=T^*e^{-(\gamma_0/V_0)(V-V^*)}, \quad \text{(C4)}$$

where T^* is the temperature at the specific volume V^* in a steady wave front. By substituting $(dP_S/dV)|_{V\text{-}V^*}$, which is obtained from Eq. (C2) with (C3), into Eq. (C1) and then replacing V^* with V, we get

$$B=-\frac{\gamma_0}{V_0}VT\left[-3Nk\left(\frac{\gamma_0}{V_0}\right)+\left(\frac{1}{2}\frac{d\Gamma}{dV}-\frac{\gamma_0}{V_0}\Gamma\right)T\right]-V\frac{dP_C}{dV}. \quad \text{(C5)}$$

[1] Y. Sano and A. Abe, J. Appl. Phys. **89**, 105 (2001).
[2] T. Sano and Y. Sano, J. Appl. Phys. **90**, 3754 (2001).
[3] D. C. Wallace, Phys. Rev. B **24**, 5597 (1981).
[4] D. C. Wallace, Phys. Rev. B **24**, 5607 (1981).
[5] J. M. Walsh and R. H. Christian, Phys. Rev. **97**, 1544 (1955).
[6] D. C. Wallace, *Thermoelastic-Plastic Flow in Solids* (LA-10119, Los Alamos National Laboratory, Los Alamos, 1985).
[7] Ya. B. Zel'dovich and Yu. P. Raizer, in *Physics of Shock Waves and High-Temperature Hydrodynamic Phenomena*, edited by W. D. Hayes and R. F. Probstein (Academic, Orlando, FL, 1966).
[8] G. E. Duvall, in *Shock Compression of Condensed Matter-1985*, edited by Y. M. Gupta (Elsevier, New York, 1986), p. 1.